ACS APPLIED MATERIALS & INTERFACES

Biological and Medical Applications of Materials and Interfaces

Identification and analysis of key parameters for the ossification on particle functionalized composites hydrogel materials.

Anatolii Abalymov, Louis Van der Meeren, Andre G Skirtach, and Bogdan V. Parakhonskiy

ACS Appl. Mater. Interfaces, **Just Accepted Manuscript** • DOI: 10.1021/acsami.0c06641 • Publication Date (Web): 15 Jun 2020

Identification and analysis of key parameters for the ossification on particle functionalized composites hydrogel materials.

Anatolii Abalymov, Louis Van der Meeren, Andre G. Skirtach, Bogdan V. Parakhonskiy*

Dept. of Biotechnology, University of Ghent, Ghent 9000, Belgium

KEYWORDS hydrogels, mineralization, particles, ossification, principal component analysis

ABSTRACT: Developing materials for tissue engineering and studying the mechanisms of cell adhesion is a complex and multifactor process that needs analysis using physical chemistry and biology. The major challenge is the labor-intensive data mining as well as requirements of the number of advanced techniques. For example, hydrogel-based biomaterials with cell-binding sites, tunable mechanical properties and complex architectures have emerged as a powerful tool to control cell adhesion and proliferation for tissue engineering. Composite hydrogels could be used for bone tissue regeneration, but they exhibit poor ossification properties. In current work, we have designed new osteoinductive gellan gum hydrogels by a thermal annealing approach and consequently functionalized them with Ca/Mg carbonates submicron particles. Determination of key parameters, which influence a successful hydroxyapatite generation, were done via the principal component analysis of 18 parameters (Young's modulus of the hydrogel and particles, particles size and mass) and cell behaviour at various time points (like viability, numbers of the cells, rate of alkaline phosphatase production and cells area) obtained by characterizing such composite hydrogel. It is determined that the particles size and concentration of calcium ions have a dominant effect on the hydroxyapatite formation, because of providing local areas with a high Young's modulus in a hydrogel – a desirable property for cell adhesion. The presented here detailed analysis allows identifying hydrogels for cell growth applications, while on the other hand, material properties can be predicted, and their overall number can be minimized leading to efficient optimization of bone reconstruction and other cell growth applications.

INTRODUCTION

One of the major goals in tissue engineering is to create artificial scaffold materials with microenvironments that trigger molecular and cellular cascade reactions.[1,2] A promising system that both enables cell adhesion and allows for the delivery of encapsulated biomolecules can be designed by incorporating particles into biomaterials and hydrogels.[3–6] But one of the major problems in such a multi-component material is analysis of parameters (mechanical (Young's modulus, stiffness, elasticity),[7] structural,[8] compositions,[9] surface properties[10]) responsible for cell adhesion, growth and proliferation,[11] and these parameters are known to be difficult to analyze, because of their interconnectivity. Besides, the interdisciplinary character of research work requires assembling such structures, where knowledge and expertise from chemistry, physics and biology are needed. Nowadays, typical methods of data analysis are based on the linear correlation between two or three parameters. For example, in one approach for PEG gel additive concentration, composition were analyzed in 20 plots.[12] And that process can be even lengthier if various compositions of gels are studied; and yet that would result in only qualitative data assessment.[13] Besides, with living systems in focus 2 or 3 parameter correlations obtained in such analysis do not represent the whole picture. One potential solution can be offered by artificial intelligence with, for example, deep learning algorithms, but that would require acquisition of extensive statistical data – a very laborious process. Therefore, identifying and analyzing key parameters leading to a prediction model is highly desirable.

Such a system can be verified on an example of hydrogels functionalized with particles, because this represents a complicated, yet very relevant and important system. The bone itself is made up of hydrogel as an organic phase consisting of collagen in the fibril form strengthened by an inorganic phase consisting of calcium-deficient hydroxyapatite.[1] Therefore, it can be regarded as a hydrogel–inorganic composite material produced by artificial mechanisms, which can fulfil both the mechanical like stiffness,[14,15] strength,[16] osteoinductivity,[17] and conductivity of the inorganic phases, and biological (cell growth and productivity) requirements in the area of tissue engineering.[18] Hence, composite hydrogels, which can be produced employing hydrogels and inorganic minerals to mimic the formation, structure, and function of natural bone tissue, are gaining particular attention.[19,20] Several hydrogels like alginate,[21] gellan gum,[13,22] collagen,[23] fibrin,[24] polyacrylamides (PA),[25] have been used as a base material for polymeric composite scaffolds. In turn, particles like a bioactive glass,[26] carbonates,[27,28]and ceramics[29] have been mainly chosen as the secondary inorganic reinforcing phase of the hydrogels, to control the properties of the composite structures. However, even though these composites provide significant advantages over single-phase structures, the development of biomaterials that effectively stimulate cell activity has yet to be finished. Osteoinductivity is only one of the many biomaterial properties, while others include physicochemical,[30] mechanical[31] and cytotoxic[32] properties. Biomaterials should provide a good environment not only for bone-derived cells or stem cells, but also for host bone cells response after in vivo implantation for consideration in the application in bone reconstruction and tissue engineering.[19] One of the most important processes involved in bone tissue formation is ossification, i.e. efficiency of hydroxyapatite (HA) production by cells.[29] One of the major factors in this process is alkaline phosphatase (ALP) molecules production by cells. ALP enzyme cut polyphosphate molecules to monophosphate.[1] Monophosphate molecules, along with ion Ca ions are building blocks of the hydroxyapatite. Different hydrogels and particles have been employed in bone implants and each system possesses its advantages and limitations, but no single-component scaffold can yet meet the demands for concurrent processability, mechanical integrity,[18] biodegradability,[33] bioactivity,[34] and osteoconductivity.[9] In this regard, it is necessary to optimize the performance of implants for bone engineering, which is taken here as an example to develop a novel method of the factor analysis as first step of machine learning algorithm application.

However, there is a gap in studies of the influence of the inorganic components on improving osteoblastic cell activity: efficiency of HA formation, ALP production, adhesion and proliferation. In pursuit of that goal, we have designed a new methodology that comprises of the consecutive thermal annealing of a gellan gum (T-A GG) precursor hydrogel and its mineralization to achieve cellular adhesion and osteogenesis stimulation by components and properties of composite hydrogels. It was hypothesized that $^{CaCO}{}_3$, Mg-enriched $^{CaCO}{}_3$ and $MgCO_3$ can affect the surface properties of the hydrogels to match the requirements of bone implants by: (I) controlling the size and morphology and chemical composition of particles through the formation of them with different mineral ratio; (II) improving the mechanical properties due to inherent stiffness of the inorganic phase; (III) influencing the bioactivity through the enhanced presence of calcium and magnesium ions which enhance ossification.

Herein, mineral-rich hydrogels (T-A GG) are produced and extensively characterized in terms of morphology, chemical compositions, thermostability, microtopography, and mechanical properties. The bioactivity potential of T-A GG mineral-reach hydrogels, as well as their capacity to promote pre-osteoblasts performance like cell density, area, level of ALP and Hap, are analyzed. The main factors affecting ossification are determined using the principal component analysis to recognize the requirements of hydrogels for successful cell adhesion and hydroxyapatite production. This is carried out in 3 steps: 1) determination of the parameters of the activity of the cells like ALP, cell density, viability cells area and their influence to the successful hydroxyapatite production; 2) estimation of parameters of the hydrogel (mechanical properties and composition influence on the successful cell adhesion, proliferation, ALP and hydroxyapatite production; 3) determination of parameters of the mineralization – the ions concentration effect on mechanical and surface properties of the hydrogels. On the basis of this analysis, the predictive capability of hydrogel design is specified.

MATERIAL AND METHOD

Synthesis of hydrogels. A solution of 3 mL, 1% (w/v) of GG (GG™ CM, Product no. G1910, 'Low-Acyl', 200–300 kDa) was placed in a petri dish with a diameter of 3.5 cm. Petri dishes with GG were placed in an oven for 4 hours at 65˚ C until complete drying. After that, 3 ml of a $CaCl_2$ (0.3 M) was applied to the surface of T-A GG. The gelation procedure lasted for 1 hour.

Samples mineralization. The hydrogel discs were mineralized by mixing of Na_2CO3 (Sigma-Aldrich), $CaCl_2$ (Sigma-Aldrich) and $MgCl_2$(Sigma Aldrich) salt solutions (dissolved in dH2O (18.2 μΩ)) in the presence of the hydrogels discs under ultrasonication (US) treatment in a US bath (Bandelin SONOREX™, Digital 10 P). For that purpose, T-A GG hydrogels discs with 3,5 cm diameter were immersed in 1 ml $CaCl_2$:$MgCl_2$ with different ratio (1:0, 0.75:0.25, 0.5:0.5, 0.25:0.75, 0:1) (0.33 M) salt solution at a container. After that, 1 ml Na_2CO_3 (0.33 M) salt solution was quickly added to the reaction mixture by pipetting at room temperature (20 ˚C ± 0.2). The sonication treatment of the reaction mixture was maintained for 60 sec. after addition of the second salt solution (Na2CO3). After the mineralization treatment, samples were removed from the reaction mixture. Then, for estimation of the dry mineral content as well as for the investigation of its crystal polymorphism and morphology, the samples were dried via a hot plate at 50 ˚C for 15 min.

Determination of sample content. Mass of the sample was controlled during treatment stages; measurements of the mass were accomplished with a Sartorius Quintix 35 (Sartorius, Germany).Attenuated total reflectance-Fourier Transform Infrared (ATR-FTIR) measurements. FTIR spectrometer, Bruker (VERTEX 70) equipped with a Platinum ATR accessory fitted with a diamond crystal, was used in experiments. The spectra are recorded in the spectral range of 150-4200 cm-1. The spectrum of each sample is measured 25 times, and the average spectrum is then calculated. The spectrum of air was taken as the background spectrum.

Scanning electron microscopy The size and shape of particles were characterized by scanning electron microscopy (SEM). Hydrogel cylinders with 5 mm diameter were cutter by biopsy and transferred to an aluminum stage covered with double-sided carbon tape. Before SEM, the hydrogels were dried under the vacuum and coated with 15 nm thick gold layer (Bal-Tec SCD050 Sputter Coater). The measurement was performed with JSM-T330A from JEOL at the operating voltage of 25 kV with secondary electrons.

X-ray diffraction X-ray diffraction (XRD) measurements were performed with Rigaku Miniflex diffractometer (Rigaku, Japan) by using CuKυ ($\lambda = 0.154$ nm) radiation source operating at 45 kV and 200 mA. The interpretation of the patterns was made with the database of the International Center of Diffraction Data (ICDD) PDF4+ was used.

Atomic force microscopy. The AFM data were acquired using A Nanowizard® 4 Atomic Force Microscope (JPK Instruments, Berlin) operated in quantitative imaging (QI®) mode (in liquid). All maps were obtained with a QP-BioAC-CI probe in (Nanosensors, Neuchâtel), using the cantilever which had a nominal frequency of 50 kHz and a force constant of 0.1 N/m (calibrated in contact-free mode). Force maps were collected using a setpoint of 3 nN at 1.6 ms per pixel, with Z length of 0.2 μm and a tip speed of 125 μm/s. The force and height maps were 20 μm by 20 μm. To measure mechanical and topographical properties, AFM was utilized with the DNP-s10 cantilever (Bruker, America).

Mechanical Tests Using an Universal Testing Machine. Mechanical stiffness of gels has been performed using a Universal Test Machine, LS1 (1 kN) Material Tester from Lloyd Instruments, Inc. (Ametek). A 50 N load cell was used for making a 0.5 mm indentation in samples with the diameter of the tip of 10 mm (the preload was set to 0.03 N).

Osteoblasts cultivation. Pre-osteoblastic MC3T3-E1 cells (ATCC) were cultured in MEM-alpha glutaMAX-1™ (Cat. No. 32561- 029) supplemented with 10% FBS, 2 mM glutamine, and 100 µg/ml penicillin/streptomycin. The media were replaced every 3 days, and the cells were maintained in a humidified incubator at 5% CO_2 and 37°C (Innova CO-170, New Brunswick Scientific).

Cells viability. The effects of mineralized scaffolds on MC3T3-E1 cells were determined by AlamarBlue (ThermoFisher Scientific) (Cat. No DAL1025). The hydrogels were placed at the bottom of the well and mineralized. MC3T3-E1 cells were seeded into 96-well cell culture plates on the mineralized hydrogel surface with at a cell density of 10×10^4 cells/well in the culture medium and incubated overnight at 37 °C under 5 % CO_2. After 24, 72 and 168 hours, 10 µL of fluorescence dye was added to each well AlamarBlue and incubated 4 hours. Fluorescent (540/610 nm) intensity was measured by a spectrophotometer (Infinite F200 PRO). The media were replaced every 3 days.

Fluorescence microscopy. To estimate a cell adhesion and proliferation on the surface of the prepared samples, viable cells were visualized by a fluorescence microscope using a microscope Nikon TI (Nik on, Japan) with Objective 4X, 10X and appropriate filters. MC3T3-E1 cells were seeded on the samples surfaces with area 0.32 cm^2 at a cell density of 10×10^4 / sample and incubated for 1, 3 and 7 days. Afterwards, cells were stained with Calcein AM. The number of cells was calculated from snapshots of three random zones for three replicates of the samples.

Alkaline Phosphatase (ALP) Activity. An enzymatic activity assay was used to measure the levels of alkaline phosphatase activity expressed from the pre-osteoblastic cells cultured on the GG hydrogels with minerals surfaces. Cells were cultured for 1, 3 and 7 days in osteogenic medium (primary medium supplemented with ascorbic acid, sodium glycerophosphate and dexamethasone (50 µg/mL, 0.1 µM, and 10 nM, respectively) and at each time point they were harvested by trypsin-EDTA and collected by centrifugation. Pellets were dissolved in 100 µL lysis buffer (0.1% Triton X-100 in 50 mM Tris-HCl pH 10.5) and were subjected to two freeze-thaw cycles from −80 °C to room temperature. Then, 100 µL of a 2 mg/mL p-nitrophenyl phosphate (pNPP, Sigma, St. Louis, MO, USA) substrate in 50 mM Tris-HCl at pH 10 with 2 mM $MgCl_2$ was added to each sample and incubated at 37 °C for 30 min. The reaction was stopped with the addition of 50 µL 1 N NaOH. Absorbance was measured using a Synergy HTX plate reader (BioTek, Winooski, VT, USA) at 405 nm and was correlated to equivalent amounts of para-nitrophenol using a calibration curve. Alkaline phosphatase activity was normalized to cellular protein levels and was measured by the Bradford assay.

HAP deposition. The extent of mineralization was determined using an Osteoimage Mineralization Assay (Lonza. Belgium.cat. no. PA-1503). After each culture time point, the hydrogels were washed with 1× PBS before being fixed with 4% (w/v) PFA for 20 min at RT. Samples were subsequently washed further twice (5–10 min each) with Osteoimage wash buffer and then incubated with 0.1 mL staining reagent, in the dark for 30 min. After incubation, gels were washed three times (5 min each) with wash buffer before. To quantify the extent of mineralization, washed samples were resuspended in 0.2-µL wash buffer and their fluorescence determined in a fluorescent plate reader (Infinite F200 PRO) at a 492/520 nm ratio. Two independent assays were performed, again in triplicates.

RESULTS

To understand the key parameters, which influence cell growth, proliferation and successful cells ossification, hydrogel matrices were in situ mineralized via various ratios of calcium and magnesium ions (Fig 1, column 1). Then, physical-chemical and mechanical properties of the hydrogel were studied in detail (Fig 1, column 2). After this, all these materials were characterized via adhesion of the osteoblastic cells, followed with studying of the cell adhesion and proliferation efficiencies like cell area, cell density and cell viability as well as the cell activity like the alkaline phosphatase production and hydroxyapatite formation. (Fig1, column3)

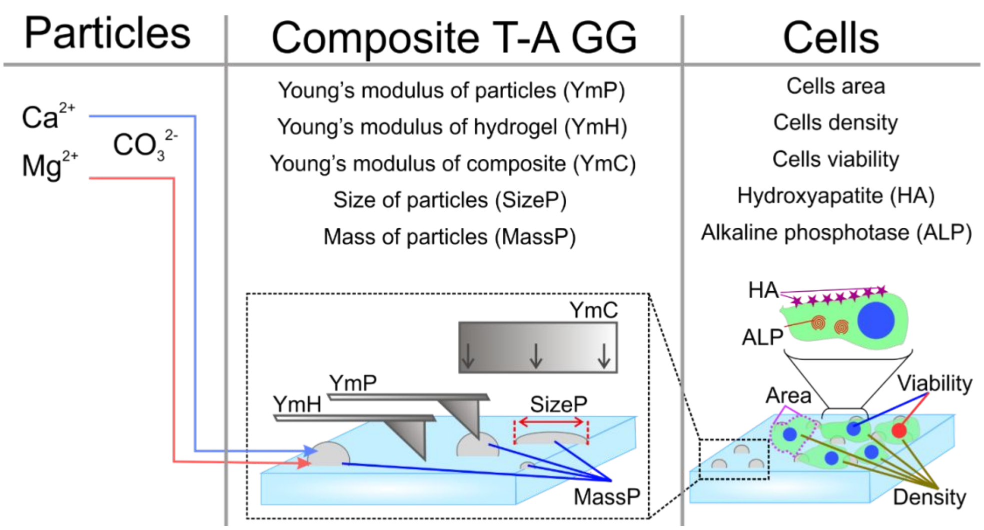

Figure 1. Schematic representation of major factors, which influenced cells ossification was analyzed. The first column represents the initial technical parameters of gel mineralisation like the ratio of the calcium and magnesium ions. The second column represents the characterization of the designed composite materials. The third column represents the factors related to the growth and activity of the cells.

The T-A GG hydrogel was produced via the thermal-annealing of the gellan gum solution; then it was gelled with Ca^{2+} ions (Figure 2a). After this gelation, the synthesis of $CaCO_3$, Mg-enriched $CaCO_3$ and $MgCO_3$ particles on the surface of the hydrogels took place by ultrasound mineralization, for which the hydrogels were placed in solutions with the corresponding ratios of $CaCl_2$, $MgCl_2$ and Na_2CO_3 solutions, **(Figure 2b-c)**. Where the amount of Na_2CO_3 was always constant (50% of total reaction mixture). The ratio of $CaCl_2$ to $MgCO_3$ was varied from 0% of $MgCl_2$ (only $CaCl_2$ and Na_2CO_3 present in reaction mixture **Figure 2b -Ca100**) to 100% of $MgCl_2$, which means only $MgCl_2$ and Na_2CO_3 were present in the reaction mixture **(Figure 2b-Ca0)**.

During mineralization, calcium or magnesium carbonate microparticles formed in the hydrogel matrix. The FTIR spectra (**Figure 2d)** prove that calcium carbonate particles were formed in samples with more than 25% of Ca^{2+} content (samples Ca25, Ca50, ca75 and Ca100). The intense absorption band at 877 cm^{-1}, which arose from out-of-plane deformation mode of CO_3^{2-}, chemically confirmed the presence of $CaCO_3$ on the T-A GG surface.

The presence of the intense band at 744 cm^{-1} corresponds to the in-plane deformation mode of CO_3^{2-} in vaterite crystals, the revealed surface was modified with porous vaterite crystals. The band at 712 cm^{-1} corresponds to bending of carbonate groups, respectively, are typical for calcium carbonate, as is the broadband at approximately 1400 cm^{-1}, corresponding to $\upsilon3$ antisymmetric stretching[35]. The samples which contained a high amount of Mg^{2+} in the reaction mixture (samples Ca50, Ca25 and Ca0) displayed a band at 714, 744 and 792 cm^{-1} corresponding to hydromagnesite ($Mg_5(CO_3)_4(OH)_2{\cdot}4H_2O$).

The major characteristic band for T-A GG is located at approximately 1030 cm^{-1}. For sample Ca25 and Ca0, the presence of the broad band at 3450 cm^{-1} corresponds to $Mg(OH)_2$. X-ray diffraction confirms these results **(Figure 2e).**

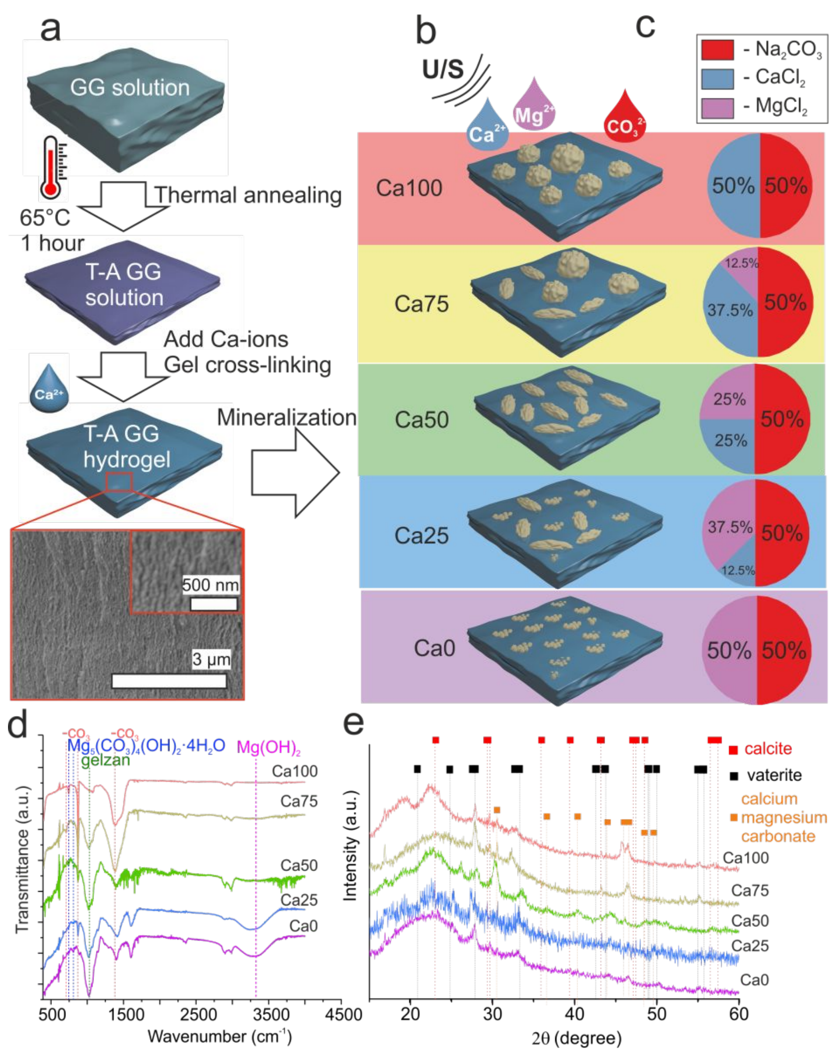

Figure 2. (a-b) Schematic representation of (a) step by step synthesis of T-A GG hydrogel (red insert is a cryo-SEM image of the internal structure of the hydrogel) and (b) formatted mineral particles after mineralization. (c) The ratio of ions in the reaction mixture. (d) FTIR spectra of GG hydrogels with different ratio of minerals. (e) X-ray diffraction spectra of GG hydrogels with different ratio of minerals.

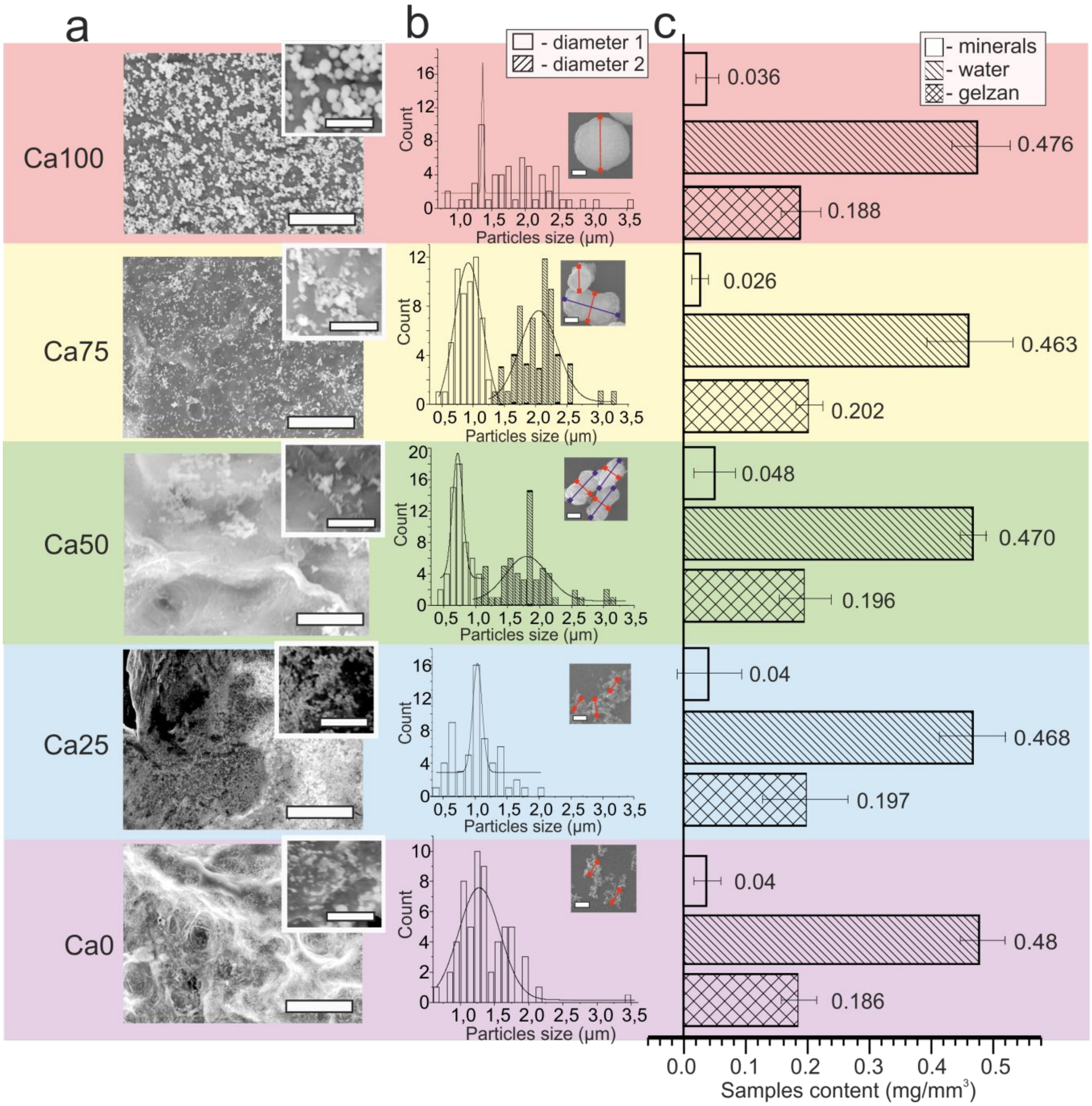

Figure 3. (a) Scanning electron microphotograph of T-A GG hydrogels pre-dried 24 hours in the oven and mineralized. Scale bar is 100 µm and 20 µm for inserts. (b) Particles size distribution on the T-A GG surface obtained by mineralization of T-A GG hydrogels. (c) Mass content of GG hydrogel with different ratio of minerals

The particle crystallographical structures were characterised using X-ray diffraction. All samples show peaks at 2θ values 27;2; 32.8; 43.9; 50.1 and 55.8; all corresponding to vaterite. Also, calcite peaks occur in these samples at 29.5 and 39.5 degrees and peak 48.2 represent of hydromagnesite and magnesium calcite.

The analysis of SEM images of minerals deposits formed on T-A GG revealed the difference between mineral structures **(Figure 3a)**. Calcium carbonate particles formed without Mg^{2+} ions in reaction mixture have a spherical shape, polycrystalline structure and exhibit a porous surface. Minerals in samples containing 25 and 50% of Mg in the reaction mixture (Ca50 and Ca75) have an ellipsoid-like polycrystal. Amorphic colloids of polycrystals of hydro-magnesite were observed in the 4th and 5th samples. The differences also related to the particle size of the minerals formed on the surface of the T-A GG **(Figure 3b)**. Polycrystals on the surface of the Ca100 sample have a diameter of around 1.8±0.5 µm. Due to the ellipsoidal form of the crystals on the Ca75 and Ca50 samples size of the long and short axis was determined.

Earlier, attempts have been made to obtain particles of calcium and magnesium carbonates with sizes from 1 till 10 microns.[36–39] Particles size usually larger and shape and morphology are quite different due to the fact that the synthesis of these particles is carried out on the surface and inside the gel matrix, which greatly affects the course of synthesis.

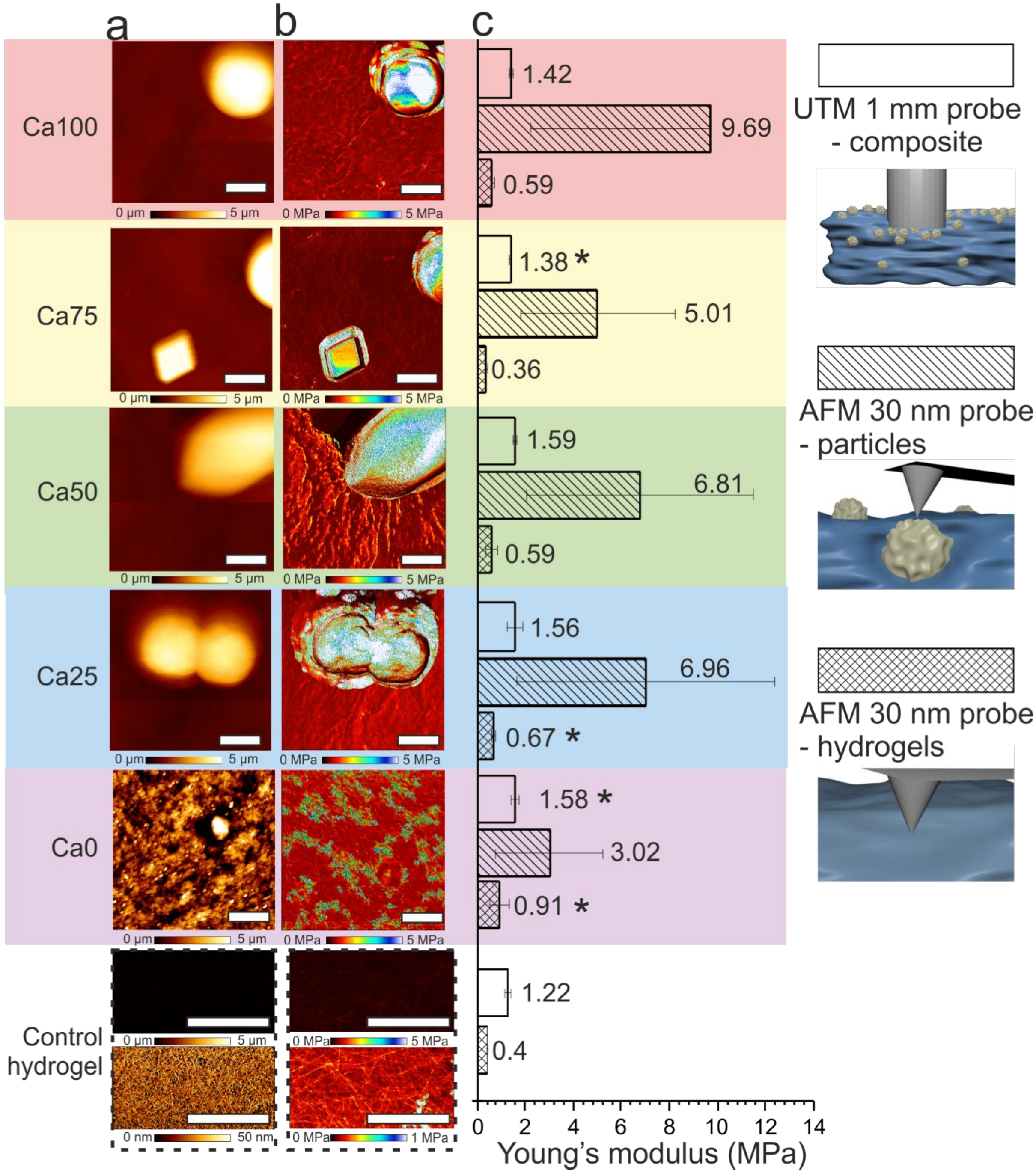

Figure 4. (a) AFM topography and (b) AFM force mapping images of T-A GG hydrogels. Scale bar is 5 um. (c) Young's modulus values for T-A GG hydrogel obtained by compression using UTM (1 mm) and AFM (30 nm) tip.

Polycrystals formed on the sample Ca75 have a large diameter of around 2.0±0.3 µm and a small diameter of approximately 0.9±0.1 µm. A decrease of Ca^{2+} ion concentration during the synthesis of sample Ca50 has obviously affected the polycrystalline size, but surface morphology remains the same. Mineral particles formed on the Ca50 samples have diameter around 1.8 ± 0.4 and diameter 2 is 0.7± 0.1 µm. It was also observed in our studies that mineral deposits are formed on the samples Ca25 and Ca0 evenly covering the surface of T-A GG by amorphous polycrystals. The diameter of these colloids of polycrystals is 0.9 ± 0.2 µm for sample Ca25 and 1.3 ± 0.4 µm for sample Ca0. The mass of water, gel and minerals in all samples was almost the same: for water, 0.47±0.01 mg/mm^3, and for the gel is 0.19±0.01 mg/mm^3 and for minerals is 0.038 ± 0.012 mg/mm^3 **(Figure 3c)**.

The influence of the mineralization of the hydrogels on mechanical properties was investigated by a compression test using a Universal Testing Machine (UTM) (to probe the Young's modulus of the composite hydrogel with a probe of diameter of 1 mm) and AFM (to map the Young's modulus of the particles and hydrogel separately, 30 nm tip).

Measurements of the Young's modulus of composite hydrogel (YmC) in the former case revealed statistically non-significant differences between control samples (control

Hydrogel) and Ca100, Ca50 and Ca25 sample:1.22, 1.42, 1.59 and 1.56 MPa, respectively **(Figure 4c)**. YmC of Ca75 and Ca0 sample of T-A GG is 1.38 MPa and 1.58 MPa. On the other hand, a more precise AFM probe allows determine separately the Young's modulus of a hydrogel area (YmH) and the Young's modulus of the particles inside hydrogel mesh (YmP). It can be seen from **Figure 4c** that some differences were observed between YmP and YmH. YmH shows more pronounced differences between control samples compare Ca25 and Ca0 sample: 0.4 MPa for control compare 0.67 MPa and 0.91. Other samples have a value of around 0.36 - 0.59MPa and don't have a significant difference compared to the control. For YmP value, none of the samples shows a significant difference due to a high standard deviation, but their Young's modulus is in the range of 3.02 to 9.69 MPa. The Ca100[t] and Ca0 samples have the highest and lowest Young's modulus.

Osteoblast cells ossification on every type of the T-A GG was studied by fluorescence microscopy, AlamarBlue assays, Hydroxyapatite (HA) deposition and alkaline phosphatase (ALP) level. Cell analysis here has been conducted on days: 1, 3, and 7 after the seeding. From fluorescence microscopy analysis we obtained qualitative properties (Figure 5a), such as the morphology of cells, and quantitative properties of cells, such as area and density, other cells parameters were obtained by spectroscopy

Cells morphology on the Ca100 and Ca75 samples is similar to the control hydrogel. We see a change in cell morphology as a n indicator of the successful cell proliferation from flattened (well, spreaded better attached to the surface cell) to more rounded (less spreaded/adhesive cell), accompanied by a decrease in the amount of calcium carbonate in the 4th and 5th samples. The cells growing on the Ca50 sample show the same morphology on the first and third day as the cells on the first and second samples, but on the seventh day, their morphology becomes the same as that on the Ca25 and Ca0 samples. This may be due to the recrystallization of carbonates on the surface of the sample. Cells growing on the Ca25 and Ca0 samples become spheroids on the seventh day of cultivation. This indicates poor adhesion properties of the composite hydrogel.

Summary of the quantitative data is presented in Figure 3-5 as a heat map (Figure 5b). To obtain a heat map, all data were normalized to the control data (cells on the cultural plastic surface) for the corresponding day. Also, the source data can be found in Table 1 in Support Information. The highest cell density was found on the Ca100 (11242 cells/cm^2) and Ca75 (11123 cells/cm^2) samples on the first day relative to the control (7376 cells/cm^2). The lowest density relative to the control (76684 cells/cm^2) is on the Ca50 (6350 cells/cm^2), Ca25 (7258 cells/cm^2) and Ca0 (4871 cells/cm^2) samples on the seventh day (Figure 5b first column).

It is also clearly seen on the heat map that the Ca50 (1064 μm^2) and Ca25 (1033 μm^2) samples on the first day have the largest cell area relative to the control (1702 μm^2). The Ca75 (836 μm^2) and Ca50 samples on the seventh day have the smallest cell area relative to the control. Cell viability on the most samples has no statistical difference in comparison with the control sample. Only samples from the Ca0 (7 days) and control hydrogel (7 days) fall out of this list and have the lowest result: 40%, and 39%, respectively.

Such a difference in viability, area, and a number of cells are in agreement with the cell adhesion on different types of particles. Obviously, cells can not adhere to Mg-rich GG hydrogels **(Figure 5a Ca25 and Ca0)**, because of particle morphology and mechanics that lead cells to gradually programmed death. This is clearly seen from result of the AlamarBlue test **(Figure 5b).**

The biosynthesis of ALP can be easily traced on the temperature map. (Figure 5b) The best synthesis of ALP occurs on samples Ca100, Ca75 and Ca0. The synthesis of hydroxyapatite is a major factor in the ossification of cells. The best result is shown by cells in sample Ca100 and Ca75 (about 500%). With a decrease in the amount of calcium in the hydrogel, the amount of hydroxyapatite decreases. However, cells that grow on a control hydrogel show a high result on the first day (459%). This may be due to calcium chloride molecules that remained in the hydrogel after the crosslinking procedure and were not used to form crystals.

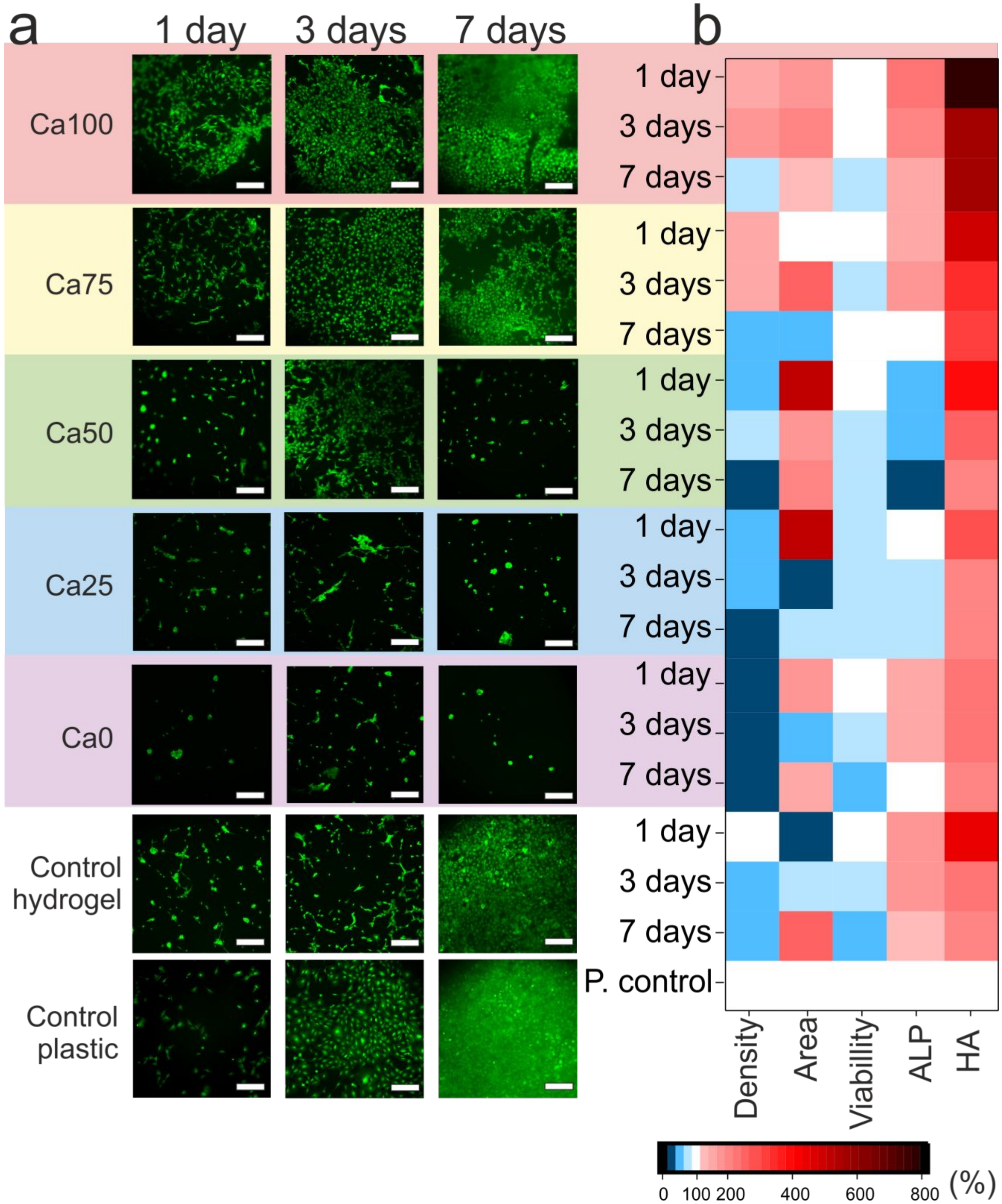

Figure 5. (a) MC3T3-E1 cells cultivated on the surface of the samples mineralized with various concentration of the calcium and magnesium ions (samples from 1to 5), control plastic and control not mineralized hydrogel during 3, 7 and 14 days (calcein, green colour). The scale bar is 200 μm. (b) heat map which represents how the difference parameter deviated from the control. The red is significantly higher than control, and the blue means significantly low then control and the white color represents the 100% control level corresponded to the plastic.

.

DISCUSSION

It is clear that multiple factors influence the rate of ossification. For analyzing the key parameters affecting hydroxyapatite production, the principal component analysis has been used. The major parameters analyzed in this study are listed in the schematics below, and the cross-correlation matrix is presented in **Table S1.**

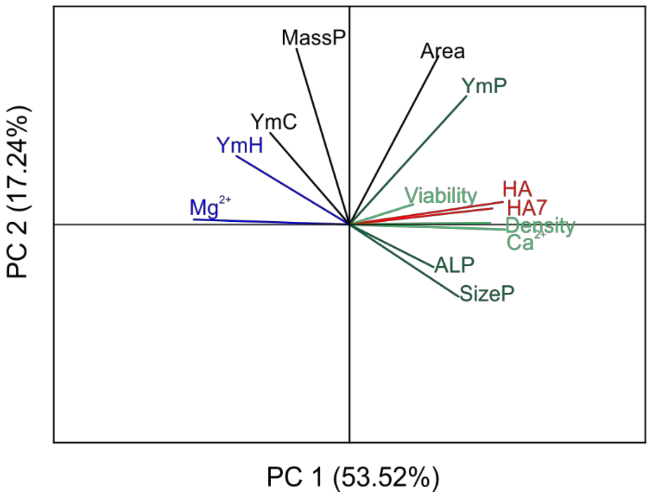

Figure 6. Factors affected by the HA production. Loading plot of the first two PC loading vectors: Mg^{2+}, Ca^{2+}, YmC, YmP, YmH, MassP, Cell area (1 day), viability (1 day), SizeP, ALP (1 day), Density, HA (1 day), HA7 (7 days). The components which represent the amount of hydroxyapatite in a first day (HA) and after the seven day (HA7) are highlighted in red color. The significance of the influence on the factor of interest are highlighted in various colors: significant positive influence (green); negative influence(blue) doesn't have a significant influence (black).

The principal component 1 (PC1) and principal component 2 (PC2) explains the variation of more than 70% of the data. The bi-plots, demonstrating how the samples are differentiated from each other, show correlations between screening parameters: the amount of HA, gel mechanical properties (YmH, YmP, YmC), cell growth efficiency (number, area, ALP, viability) **(Figure 6)**. In 2-dimensional PCA bi-plots, the lengths of the vectors estimate the standard deviations of the respective variables and the cosine values of angles between vectors approximating the intervariable correlations[40]**.** The components, which have a positive influence, have a smaller angle (highlights with green). It can be clarified that the major factors correlated with the amount of the HA after one week (HA7) is the amount of HA in the first day as well as the cells viability, cells number and the percentage of calcium in reaction synthesis. It means that all initial cell parameters, except the cell area, are positively influenced by the long-term efficiency of the HA production. In regard to gel properties, just the Young's modulus of the particles and size of the particles have a correlation.

Therefore, in the next step, we identify the factors influencing the initial cell growth and adhesion **(Figure 7a-e)**. We are interested in studying the following cell parameters: 1) density; 2) area; 3) viability **(Figure 7).** In regard with all initial cell parameters, sizeP and YmP have a stronger influence. But for the area occupied by cells, the massP and the presence of Ca^{2+} are key factors. Its means that cells prefer to grow on larger particles, which are fixed in the hydrogel structure and provide the highest Young's modulus. Since Ca^{2+} ions are a part of HA, increasing more calcium-based structures (the calcium carbonate rather than calcium magnesite) could have an influence on the HA formation as well. On the other hand, such additional parameters as the presence of the Mg^{2+} ions and YmH have a negative influence on the formation of HA **(Figure 7e)**. This can be due to the inverse correlation of these parameters with Ca^{2+}. Mg-rich particles doesn't toxic by themself. [39,41–43] But in our case morphology and mechanical properties of the particles have critical influence to the density of adhered cell **(Figure 7a),** and as result to cell viability **(Figure 7c)**.

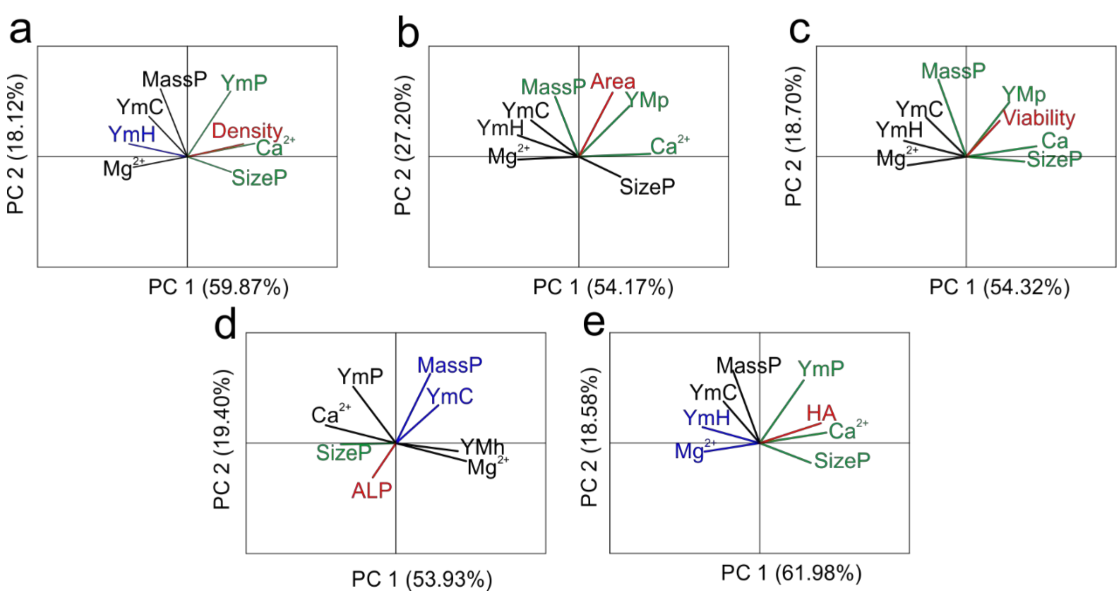

Figure 7. Loading plot of the first two PC loading vectors: Mg^{2+}, Ca^{2+}, YmC, YmP, YmH, MassP, Area, Viability, SizeP, ALP, Density, HA. In red color highlighted the factor of interest. The significance of the influence on the factor of interest is highlighted in various colors: significant positive influence (green); negative influence(blue) doesn't have a significant influence (black).

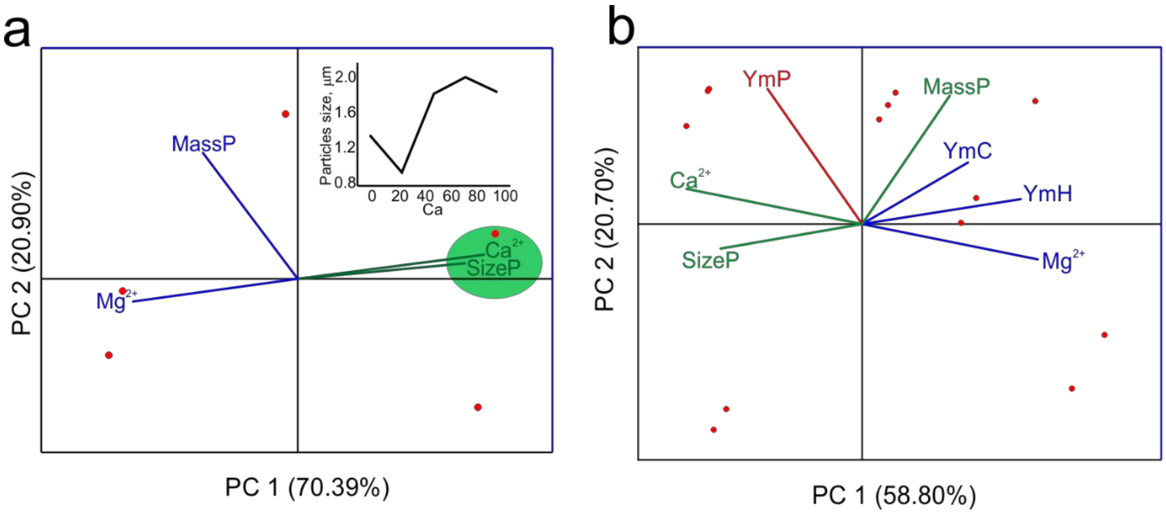

Figure 8. Loading plot of the first two principal component loading vectors: a) Mg^{2+}, Ca^{2+}, SizeP and MassP b) YmC, YmP, YmH, MassP, SizeP, Mg^{2+}, Ca^{2+}. The factor of interest is highlighted in red color. The significance of the influence on the factor of interest is highlighted in various colors: significant positive influence (green); negative influence(blue) doesn't have a significant influence (black). Inset in figure 8a demonstrates the correlation between the particle size and the percentage of calcium ions in the reaction mixture.

Since the sizeP and YmP are the key parameters for HA production, we determine which factors affect them **(Figure 8a)**. The percentage of Ca^{2+} ions has a significant influence on the sizeP and doesn't have an influence on the massP. Consequently, there is an influence of the sizeP, massP and Ca^{2+} on the YmP **(Figure 8b)**. Furthermore, one can notice that the YmC is a combination of the YmH and YmP. But such an integral characterization obtained by the universal testing machine doesn't provide sufficient information for such a composite material.

In our case, more Ca^{2+} in synthesis provides vaterite particles with a larger size and less amorphous phase. Therefore, they are more stable in the gel and provide the highest YmP. Analysis of **Figure 6** demonstrates that YmP has a key influence on the growth of cells due to better adherence of cells to the particles. In other words, cells grab them more efficient larger particles, which are fixed in the gel. For this reason, the number of cells, their viability, production of ALP and HA increases significantly. Therefore, in order to provide an efficient HA formation, the presence of the Ca^{2+} ions is needed, which is an inherent a part of HA, thus this could be influenced directly (as a part of the HA structure) and indirectly through the formation of more stable, large particles providing a relatively high Young's modulus.

Having carried out the analysis above, a question arises: how applicable is the described above approach to other types of hydrogels and particles? We have found that the general patterns can be extended beyond gellan gum and Ca/Mg carbonate particles, and they could thus be of a more universal nature. For example, alginate hydrogel mineralized by calcium carbonate particles[44] demonstrates that particles are the driving mechanism of cell adhesion to hydrogels. Furthermore, the ideas of particles influencing the cell adhesion could be extended to such pre-synthesized colloid ceramic particles as silica, calcium carbonate (in the vaterite form).[21] Moreover, it is shown that particle morphology is the key factor in cell adhesion, since porous calcium carbonate exhibited a significantly higher cell adhesion than smooth silica particles. [44] In regard with various types of gels including alginate or gellan gum or just metal surfaces: calcium carbonate particles play an important role in ossification,: it can be both a container for carrying ossification, thus accelerating enzymes, or a material applied to build a hydroxyapatite matrix.[45]

CONCLUSION

In conclusion, we have determined key parameters of hydrogel-based composite materials i*n situ* functionalized with calcium carbonate and magnesium carbonate particles stimulating the ossification. First, biological and physical chemistry processes behind the ossification process were studied. Second, we have determined key parameters with the focus on data mining procedure to formulate and train the prediction model, which would describe repeatable gel formulations for osteoblastic cell growth. Variation of such hydrogel mineralization factors as the ratio of Ca^{2+} and Mg^{2+} ions in the reaction mixture, the influence of the cell area, viability, density, ALP production, and HA formation were analyzed. This occurs upon changing parameters such as the size of particles, the mass of minerals, mechanical properties of the hydrogel, particles and their composite. In addition, a number of material parameters and complex cellular behavior were analyzed via principal component analysis and key factors of materials, which act on a particular cellular trait, were determined. In this case, a higher amount of Ca^{2+} in the reaction mixture (100 and 75%) produce vaterite particles with a larger size, around 1.8 ± 0.5 µm, and to a lesser degree the amorphous phase. Therefore, they are better fixed in the gel structure and provide the highest Young's modulus (9.69 MPa). For efficient cell growth, just YmP is more important since cells can adhere better to the particles. It was observed that cells adhere better to materials functionalized with larger particles, because these particles need to be well fixed in the hydrogel matrix. Furthermore, cells proliferate 12 times faster on Ca ions rich hydrogel, and their viability is 2 times higher than that for Mg-rich hydrogels after 7 days of incubation, which is the main factor influencing the formation of hydroxyappatite (3 times higher). As a generalization of this research, the reported dependence of cell adhesion on various materials can be also extended to other types of gels and particles.

ASSOCIATED CONTENT

Supporting Information

The support information contained the table with original data form experiment data.xls. The Supporting Information is available free of charge on the ACS Publications website.

AUTHOR INFORMATION

Corresponding Author

* Bogdan.Parakhonkiy@UGent.be

Author Contributions

The manuscript was written through contributions of all authors. / All authors have given approval to the final version of the manuscript.

Funding Sources

AA thanks the “Global education” program of the Russian government for funding. BVP is FWO post-doctoral fellow. This research is supported by the Special Research Fund (BOF) of Ghent University (01IO3618, BAS094-18, BOF14/IOP/003) and FWO-Vlaanderen (G043219, 1524618N, G0D7115N).

ACKNOWLEDGMENT

(AA thanks the “Global education” program of the Russian government for funding. BVP is FWO post-doctoral fellow. This research is supported by the Special Research Fund (BOF) of Ghent University (01IO3618, BAS094-18, BOF14/IOP/003) and FWO-Vlaanderen (G043219, 1524618N).

REFERENCES

(1) Reznikov, N.; Steele, J. A. M.; Fratzl, P.; Stevens, M. M. A Materials Science Vision of Extracellular Matrix Mineralization. *Nat. Rev. Mater.* **2016**, *1* (8), 16041. https://doi.org/10.1038/natrevmats.2016.41.

(2) Miar, S.; Shafiee, A.; Guda, T.; Narayan, R. Additive Manufacturing for Tissue Engineering. In *3D Printing and Biofabrication*; Springer International Publishing: Cham, 2018; pp 1–52. https://doi.org/10.1007/978-3-319-40498-1_2-1.

(3) Mitrousis, N.; Fokina, A.; Shoichet, M. S. Biomaterials for Cell Transplantation. *Nat. Rev. Mater.* **2018**, *3* (11), 441–456. https://doi.org/10.1038/s41578-018-0057-0.

(4) Yesildag, C.; Ouyang, Z.; Zhang, Z.; Lensen, M. C. Micro-Patterning of PEG-Based Hydrogels with Gold Nanoparticles Using a Reactive Micro-Contact-Printing Approach. *Front. Chem.* **2019**, *7* (JAN), 1–10. https://doi.org/10.3389/fchem.2018.00667.

(5) Lee, K. Y.; Mooney, D. J. Alginate: Properties and Biomedical Applications. *Prog. Polym. Sci.* **2012**, *37* (1), 106–126. https://doi.org/10.1016/j.progpolymsci.2011.06.003.

(6) Abalymov, A.; Parakhonskiy, B.; Skirtach, A. G. Polymer- and Hybrid-Based Biomaterials for Interstitial, Connective, Vascular, Nerve, Visceral and Musculoskeletal Tissue Engineering. *Polymers (Basel).* **2020**, *12* (3), 620. https://doi.org/10.3390/polym12030620.

(7) Li, L.; Eyckmans, J.; Chen, C. S. Designer Biomaterials for Mechanobiology. *Nat. Mater.* **2017**, *16* (12), 1164–1168. https://doi.org/10.1038/nmat5049.

(8) Marmorat, C.; Arinstein, A.; Koifman, N.; Talmon, Y.; Zussman, E.; Rafailovich, M. Cryo-Imaging of Hydrogels Supermolecular Structure. *Sci. Rep.* **2016**, *6* (May), 6–11. https://doi.org/10.1038/srep25495.

(9) Ingavle, G. C.; Gionet-Gonzales, M.; Vorwald, C. E.; Bohannon, L. K.; Clark, K.; Galuppo, L. D.; Leach, J. K. Injectable Mineralized Microsphere-Loaded Composite Hydrogels for Bone Repair in a Sheep Bone Defect Model. *Biomaterials* **2019**, *197* (August 2018), 119–128. https://doi.org/10.1016/j.biomaterials.2019.01.005.

(10) Gittens, R. A.; Scheideler, L.; Rupp, F.; Hyzy, S. L.; Geis-Gerstorfer, J.; Schwartz, Z.; Boyan, B. D. A Review on the Wettability of Dental Implant Surfaces II: Biological and Clinical Aspects. *Acta Biomater.* **2014**, *10* (7), 2907–2918. https://doi.org/10.1016/j.actbio.2014.03.032.

(11) Geiger, B.; Spatz, J. P.; Bershadsky, A. D. Environmental Sensing through Focal Adhesions. *Nat. Rev. Mol. Cell Biol.* **2009**, *10* (1), 21–33. https://doi.org/10.1038/nrm2593.

(12) Nam, S.; Stowers, R.; Lou, J.; Xia, Y.; Chaudhuri, O. Varying PEG Density to Control Stress Relaxation in Alginate-PEG Hydrogels for 3D Cell Culture Studies. *Biomaterials* **2019**, *200*, 15–24. https://doi.org/10.1016/j.biomaterials.2019.02.004.

(13) Douglas, T. E. L.; Łapa, A.; Samal, S. K.; Declercq, H. A.; Schaubroeck, D.; Mendes, A. C.; der Voort, P. Van; Dokupil, A.; Plis, A.; De Schamphelaere, K.; Chronakis, I. S.; Pamuła, E.; Skirtach, A. G. Enzymatic, Urease-Mediated Mineralization of Gellan Gum Hydrogel with Calcium Carbonate, Magnesium-Enriched Calcium Carbonate and Magnesium Carbonate for Bone Regeneration Applications. *J. Tissue Eng. Regen. Med.* **2017**, *11* (12), 3556–3566. https://doi.org/10.1002/term.2273.

(14) Vining, K. H.; Mooney, D. J. Mechanical Forces Direct Stem Cell Behaviour in Development and Regeneration. *Nat. Rev. Mol. Cell Biol.* **2017**, *18* (12), 728–742. https://doi.org/10.1038/nrm.2017.108.

(15) Discher, D. E.; Janmey, P.; Wang, Y. L. Tissue Cells Feel and Respond to the Stiffness of Their Substrate. *Science (80-.).* **2005**, *310* (5751), 1139–1143. https://doi.org/10.1126/science.1116995.

(16) Huebsch, N.; Lippens, E.; Lee, K.; Mehta, M.; Koshy, S. T.; Darnell, M. C.; Desai, R. M.; Madl, C. M.; Xu, M.; Zhao, X.; Chaudhuri, O.; Verbeke, C.; Kim, W. S.; Alim, K.; Mammoto, A.; Ingber, D. E.; Duda, G. N.; Mooney, D. J. Matrix Elasticity of Void-Forming Hydrogels Controls Transplanted-Stem-Cell-Mediated Bone Formation. *Nat. Mater.* **2015**, *14* (12), 1269–1277. https://doi.org/10.1038/nmat4407.

(17) García-Gareta, E.; Coathup, M. J.; Blunn, G. W. Osteoinduction of Bone Grafting Materials for Bone Repair and Regeneration. *Bone* **2015**, *81*, 112–121. https://doi.org/10.1016/j.bone.2015.07.007.

(18) Saveleva, M. S.; Eftekhari, K.; Abalymov, A.; Douglas, T. E. L.; Volodkin, D.; Parakhonskiy, B. V.; Skirtach, A. G. Hierarchy of Hybrid Materials—The Place of Inorganics-in-Organics in It, Their Composition and Applications. *Front. Chem.* **2019**, *7*. https://doi.org/10.3389/fchem.2019.00179.

(19) Zhang, K.; Wang, S.; Zhou, C.; Cheng, L.; Gao, X.; Xie, X.; Sun, J.; Wang, H.; Weir, M. D.; Reynolds, M. A.; Zhang, N.; Bai, Y.; Xu, H. H. K. Advanced Smart Biomaterials and Constructs for Hard Tissue Engineering and Regeneration. *Bone Res.* **2018**, *6* (1), 31. https://doi.org/10.1038/s41413-018-0032-9.

(20) Gao, C.; Peng, S.; Feng, P.; Shuai, C. Bone Biomaterials and Interactions with Stem Cells. *Bone Res.* **2017**, *5* (1), 17059. https://doi.org/10.1038/boneres.2017.59.

(21) Muderrisoglu, C.; Saveleva, M.; Abalymov, A.; Van der Meeren, L.; Ivanova, A.; Atkin, V.; Parakhonskiy, B.; Skirtach, A. G. Nanostructured Biointerfaces Based on Bioceramic Calcium Carbonate/Hydrogel Coatings on Titanium with an Active Enzyme for Stimulating Osteoblasts Growth. *Adv. Mater. Interfaces* **2018**, *5* (19), 1800452. https://doi.org/10.1002/admi.201800452.

(22) Zia, K. M.; Tabasum, S.; Khan, M. F.; Akram, N.; Akhter, N.; Noreen, A.; Zuber, M. Recent Trends on Gellan Gum Blends with Natural and Synthetic Polymers: A Review. *Int. J. Biol. Macromol.* **2018**, *109*, 1068–1087. https://doi.org/10.1016/j.ijbiomac.2017.11.099.

(23) Yan, H.; Huang, D.; Chen, X.; Liu, H.; Feng, Y.; Zhao, Z.; Dai, Z.; Zhang, X.; Lin, Q. A Novel and Homogeneous Scaffold Material: Preparation and Evaluation of Alginate/Bacterial Cellulose Nanocrystals/Collagen Composite Hydrogel for Tissue

Engineering. *Polym. Bull.* **2018**, *75* (3), 985–1000. https://doi.org/10.1007/s00289-017-2077-0.

(24) Noori, A.; Ashrafi, S. J.; Vaez-Ghaemi, R.; Hatamian-Zaremi, A.; Webster, T. J. A Review of Fibrin and Fibrin Composites for Bone Tissue Engineering. *Int. J. Nanomedicine* **2017**, *12*, 4937–4961. https://doi.org/10.2147/IJN.S124671.

(25) Fang, J.; Li, P.; Lu, X.; Fang, L.; Lü, X.; Ren, F. A Strong, Tough, and Osteoconductive Hydroxyapatite Mineralized Polyacrylamide/Dextran Hydrogel for Bone Tissue Regeneration. *Acta Biomater.* **2019**, *88*, 503–513. https://doi.org/10.1016/j.actbio.2019.02.019.

(26) Zeng, Q.; Desai, M. S.; Jin, H.-E.; Lee, J. H.; Chang, J.; Lee, S.-W. Self-Healing Elastin–Bioglass Hydrogels. *Biomacromolecules* **2016**, *17* (8), 2619–2625. https://doi.org/10.1021/acs.biomac.6b00621.

(27) Douglas, T. E. L.; Sobczyk, K.; Łapa, A.; Włodarczyk, K.; Brackman, G.; Vidiasheva, I.; Reczyńska, K.; Pietryga, K.; Schaubroeck, D.; Bliznuk, V.; Voort, P. Van Der; Declercq, H. A.; Bulcke, J. Van den; Samal, S. K.; Khalenkow, D.; Parakhonskiy, B. V.; Van Acker, J.; Coenye, T.; Lewandowska-Szumieł, M.; Pamuła, E.; Skirtach, A. G. Ca:Mg:Zn:CO 3 and Ca:Mg:CO 3 —Tri- and Bi-Elemental Carbonate Microparticles for Novel Injectable Self-Gelling Hydrogel–Microparticle Composites for Tissue Regeneration. *Biomed. Mater.* **2017**, *12* (2), 025015. https://doi.org/10.1088/1748-605X/aa6200.

(28) Douglas, T. E. L.; Messersmith, P. B.; Chasan, S.; Mikos, A. G.; de Mulder, E. L. W.; Dickson, G.; Schaubroeck, D.; Balcaen, L.; Vanhaecke, F.; Dubruel, P.; Jansen, J. A.; Leeuwenburgh, S. C. G. Enzymatic Mineralization of Hydrogels for Bone Tissue Engineering by Incorporation of Alkaline Phosphatase. *Macromol. Biosci.* **2012**, *12* (8), 1077–1089. https://doi.org/10.1002/mabi.201100501.

(29) Wang, W.; Yeung, K. W. K. Bone Grafts and Biomaterials Substitutes for Bone Defect Repair: A Review. *Bioact. Mater.* **2017**, *2* (4), 224–247. https://doi.org/10.1016/j.bioactmat.2017.05.007.

(30) Mitić, Ž.; Stolić, A.; Stojanović, S.; Najman, S.; Ignjatović, N.; Nikolić, G.; Trajanović, M. Instrumental Methods and Techniques for Structural and Physicochemical Characterization of Biomaterials and Bone Tissue: A Review. *Mater. Sci. Eng. C* **2017**, *79*, 930–949. https://doi.org/10.1016/j.msec.2017.05.127.

(31) Zhang, X. Y.; Fang, G.; Zhou, J. Additively Manufactured Scaffolds for Bone Tissue Engineering and the Prediction of Their Mechanical Behavior: A Review. *Materials (Basel).* **2017**, *10* (1), 50. https://doi.org/10.3390/ma10010050.

(32) Torres, M. L.; Fernandez, J. M.; Dellatorre, F. G.; Cortizo, A. M.; Oberti, T. G. Purification of Alginate Improves Its Biocompatibility and Eliminates Cytotoxicity in Matrix for Bone Tissue Engineering. *Algal Res.* **2019**, *40*, 101499. https://doi.org/10.1016/j.algal.2019.101499.

(33) Caliari, S. R.; Burdick, J. A. A Practical Guide to Hydrogels for Cell Culture. *Nat. Methods* **2016**, *13* (5), 405–414. https://doi.org/10.1038/nmeth.3839.

(34) Seo, M.; Seo, M.; Choi, S. E.; Shin, K.; Lee, J. B.; Yang, D. Y.; Kim, J. W. Cellulose Nanofiber-Multilayered Fruit Peel-Mimetic Gelatin Hydrogel Microcapsules for Micropackaging of Bioactive Ingredients. *Carbohydr. Polym.* **2020**, *229*, 115559. https://doi.org/10.1016/j.carbpol.2019.115559.

(35) Andersen, F. A.; Brečević, L.; Beuter, G.; Dell'Amico, D. B.; Calderazzo, F.; Bjerrum, N. J.; Underhill, A. E. Infrared Spectra of Amorphous and Crystalline Calcium Carbonate. *Acta Chem. Scand.* **1991**, *45*, 1018–1024. https://doi.org/10.3891/acta.chem.scand.45-1018.

(36) Svenskaya, Y. I.; Fattah, H.; Inozemtseva, O. A.; Ivanova, A. G.; Shtykov, S. N.; Gorin, D. A.; Parakhonskiy, B. V. Key Parameters for Size- and Shape-Controlled Synthesis of Vaterite Particles. *Cryst. Growth Des.* **2018**, *18* (1), 331–337. https://doi.org/10.1021/acs.cgd.7b01328.

(37) Svenskaya, Y. I.; Fattah, H.; Zakharevich, A. M.; Gorin, D. A.; Sukhorukov, G. B.; Parakhonskiy, B. V. Ultrasonically Assisted Fabrication of Vaterite Submicron-Sized Carriers. *Adv. Powder Technol.* **2016**, *27* (2), 618–624. https://doi.org/10.1016/j.apt.2016.02.014.

(38) Douglas, T. E. L.; Łapa, A.; Samal, S. K.; Declercq, H. A.; Schaubroeck, D.; Mendes, A. C.; der Voort, P. Van; Dokupil, A.; Plis, A.; De Schamphelaere, K.; Chronakis, I. S.; Pamuła, E.; Skirtach, A. G. Enzymatic, Urease-Mediated Mineralization of Gellan Gum Hydrogel with Calcium Carbonate, Magnesium-Enriched Calcium Carbonate and Magnesium Carbonate for Bone Regeneration Applications. *J. Tissue Eng. Regen. Med.* **2017**, *11* (12), 3556–3566. https://doi.org/10.1002/term.2273.

(39) Douglas, T. E. L.; Łapa, A.; Reczyńska, K.; Krok-Borkowicz, M.; Pietryga, K.; Samal, S. K.; Declercq, H. A.; Schaubroeck, D.; Boone, M.; Van der Voort, P.; De Schamphelaere, K.; Stevens, C. V.; Bliznuk, V.; Balcaen, L.; Parakhonskiy, B. V.; Vanhaecke, F.; Cnudde, V.; Pamuła, E.; Skirtach, A. G. Novel Injectable, Self-Gelling Hydrogel–Microparticle Composites for Bone Regeneration Consisting of Gellan Gum and Calcium and Magnesium Carbonate Microparticles. *Biomed. Mater.* **2016**, *11* (6), 065011. https://doi.org/10.1088/1748-6041/11/6/065011.

(40) Aitchison, J.; Greenacre, M. Biplots of Compositional Data. *J. R. Stat. Soc. Ser. C Appl. Stat.* **2002**, *51* (4), 375–392. https://doi.org/10.1111/1467-9876.00275.

(41) Rezaei, M.; Tamjid, E.; Dinari, A. Enhanced Cell Attachment and Hemocompatibility of Titanium by Nanoscale Surface Modification through Severe Plastic Integration of Magnesium-Rich Islands and Porosification. *Sci. Rep.* **2017**, *7* (1), 12965. https://doi.org/10.1038/s41598-017-13169-7.

(42) Kirkland, N. T.; Birbilis, N.; Staiger, M. P. Assessing the Corrosion of Biodegradable Magnesium Implants: A Critical Review of Current Methodologies and Their Limitations. *Acta Biomater.* **2012**, *8* (3), 925–936. https://doi.org/10.1016/j.actbio.2011.11.014.

(43) Park, J.-W.; Kim, Y.-J.; Jang, J.-H.; Song, H. Osteoblast Response to Magnesium Ion-Incorporated Nanoporous Titanium Oxide Surfaces. *Clin. Oral Implants Res.* **2010**, *21* (11), 1278–1287. https://doi.org/10.1111/j.1600-0501.2010.01944.x.

(44) Abalymov, A.; Van der Meeren, L.; Saveleva, M.; Prikhozhdenko, E.; Dewettinck, K.; Parakhonskiy, B. V.; Skirtach, A. G. Cells-Grab-on Particles – a Novel Approach to Control Cell Focal Adhesion on Hybrid Hydrogels. *ACS Biomater. Sci. Eng.* **2020**, acsbiomaterials.0c00119. https://doi.org/10.1021/acsbiomaterials.0c00119.

(45) Abalymov, A.; Van Poelvoorde, L.; Atkin, V. S.; Skirtach, A. G.; Konrad, M.; Parakhonskiy, B. Alkaline Phosphatase Delivery System Based on Calcium Carbonate Carriers for Acceleration of Ossification. *ACS Appl. Bio Mater.* **2020**, acsabm.0c00053. https://doi.org/10.1021/acsabm.0c00053.

SYNOPSIS TOC.

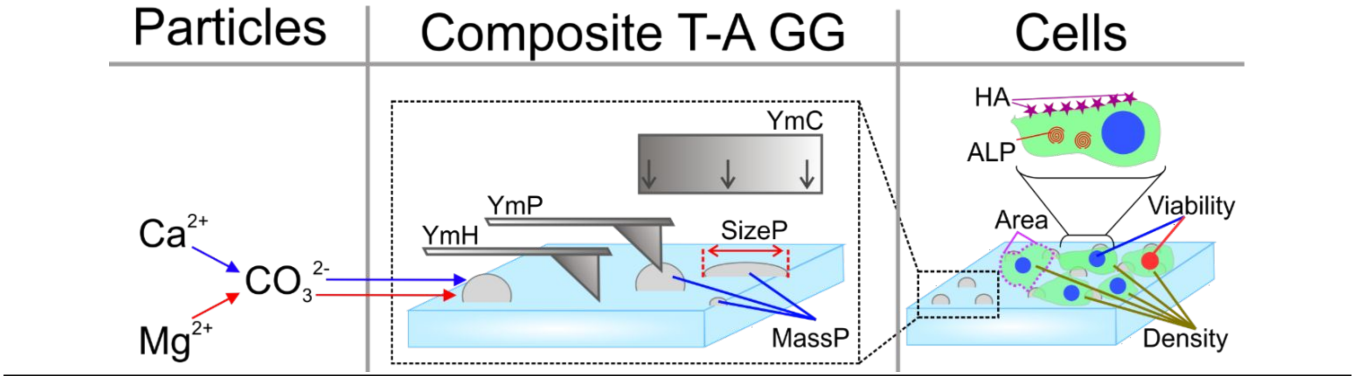

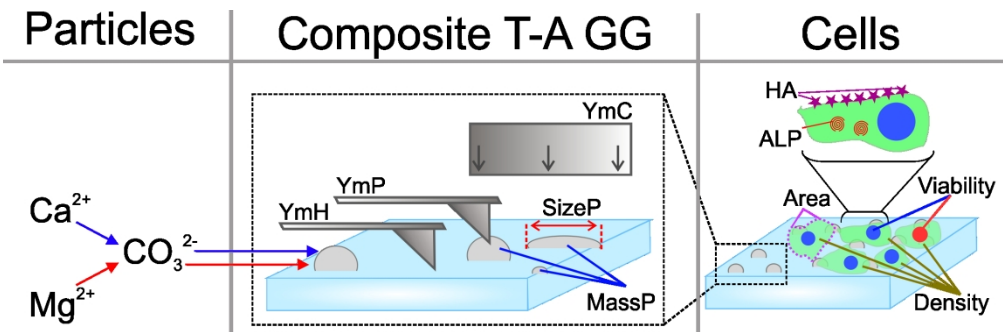

table of content

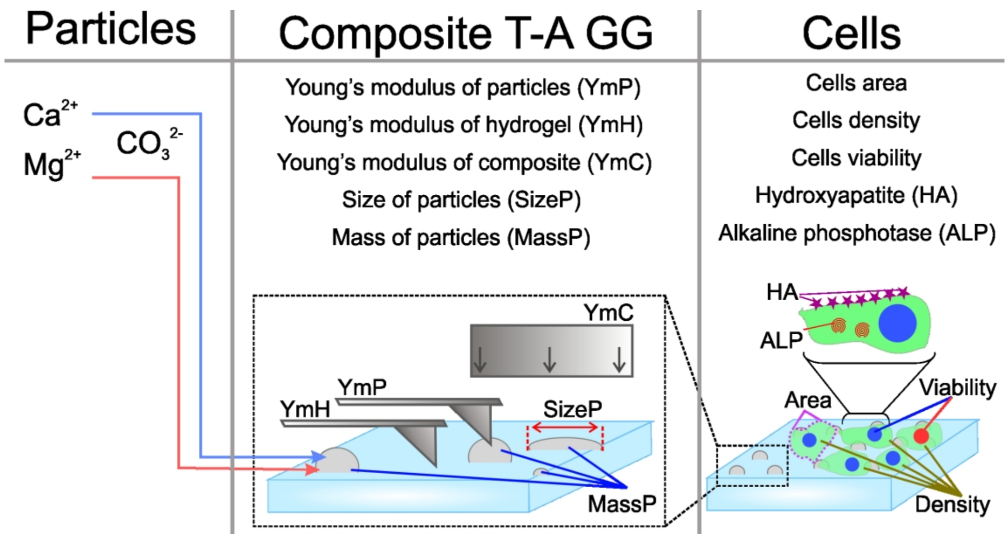

Figure 1. Schematic representation of major factors, which influenced cells ossification was analyzed. The first column represents the initial technical parameters of gel mineralisation like the ratio of the calcium and magnesium ions. The second column represents the characterization of the designed composite materials. The third column represents the factors related to the growth and activity of the cells.

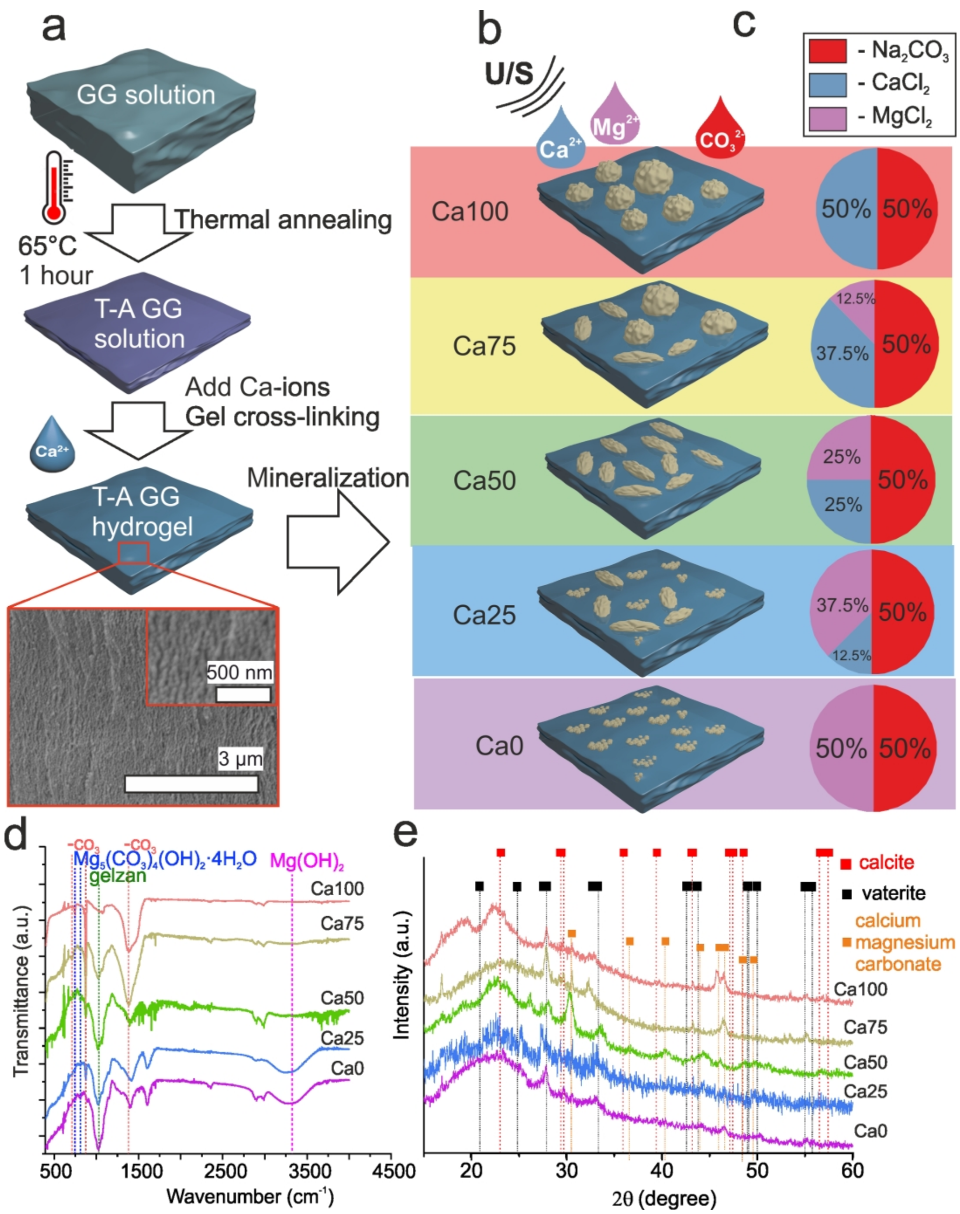

Figure 2. (a-b) Schematic representation of (a) step by step synthesis of T-A GG hydrogel (red insert is a cryo-SEM image of the internal structure of the hydrogel) and (b) formatted mineral particles after mineralization. (c) The ratio of ions in the reaction mixture. (d) FTIR spec-tra of GG hydrogels with different ratio of minerals. (e) X-ray diffraction spectra of GG hydrogels with different ratio of minerals.

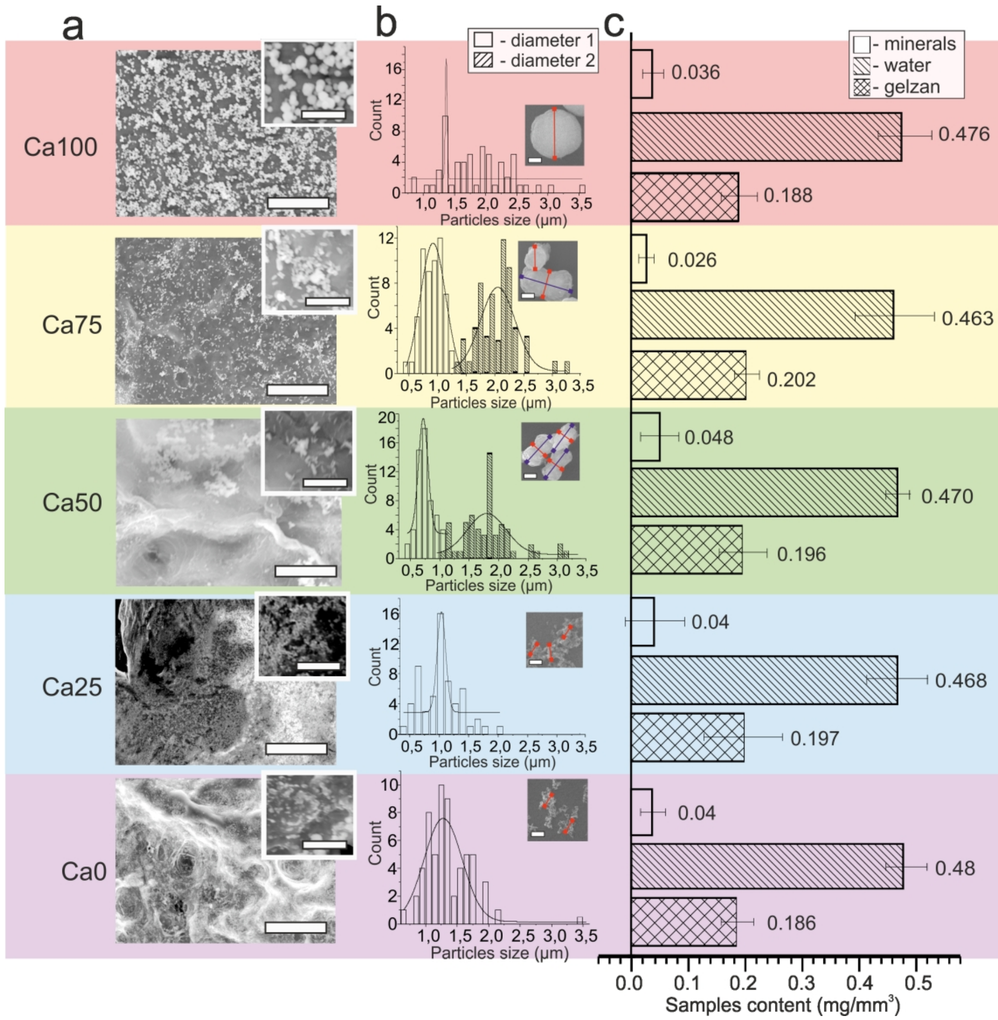

Figure 3. (a) Scanning electron microphotograph of T-A GG hydrogels pre-dried 24 hours in the oven and mineralized. Scale bar is 100 µm and 20 µm for inserts. (b) Particles size distribution on the T-A GG surface obtained by mineralization of T-A GG hydrogels. (c) Mass con-tent of GG hydrogel with different ratio of minerals

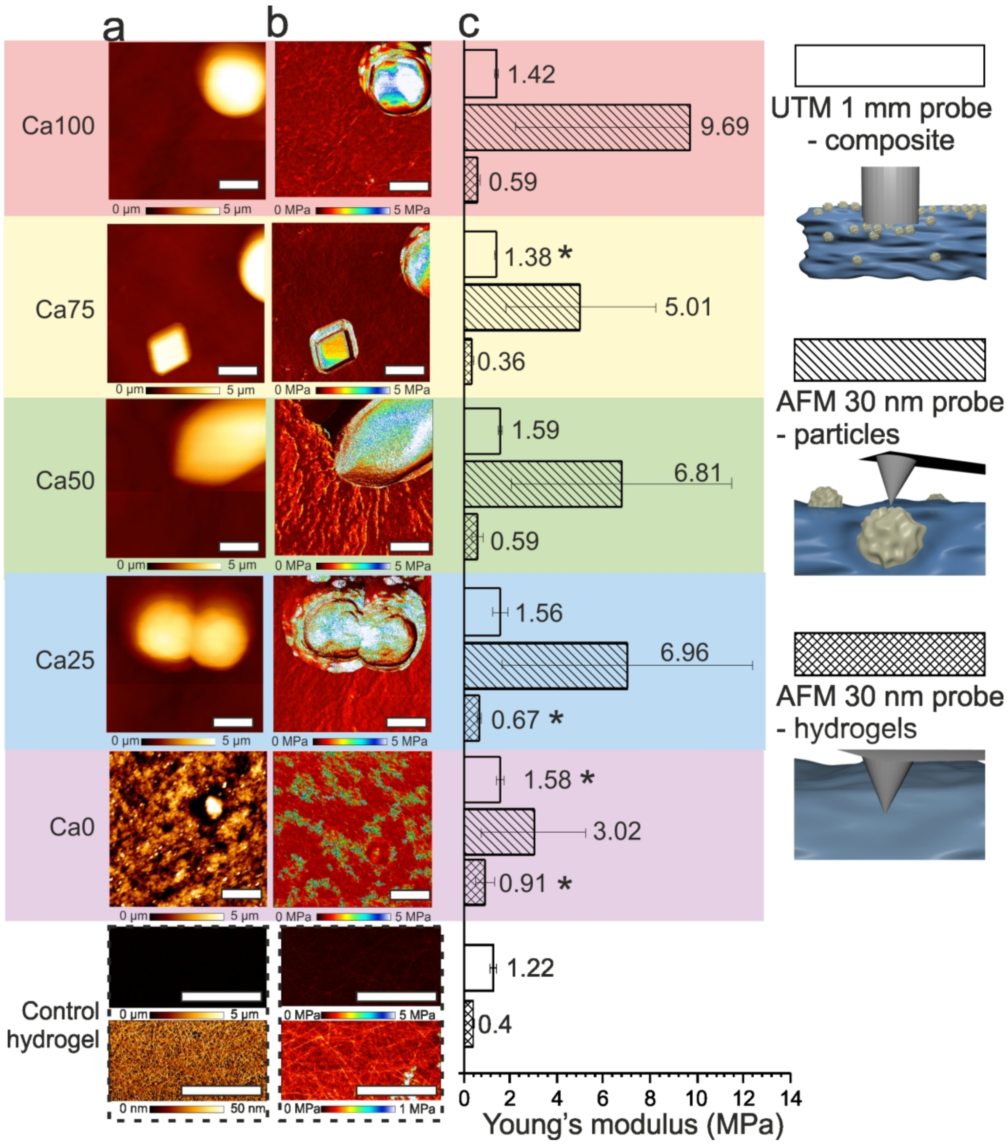

Figure 4. (a) AFM topography and (b) AFM force mapping images of T-A GG hydrogels. Scale bar is 5 um. (c) Young's modulus values for T-A GG hydrogel obtained by compression using UTM (1 mm) and AFM (30 nm) tip

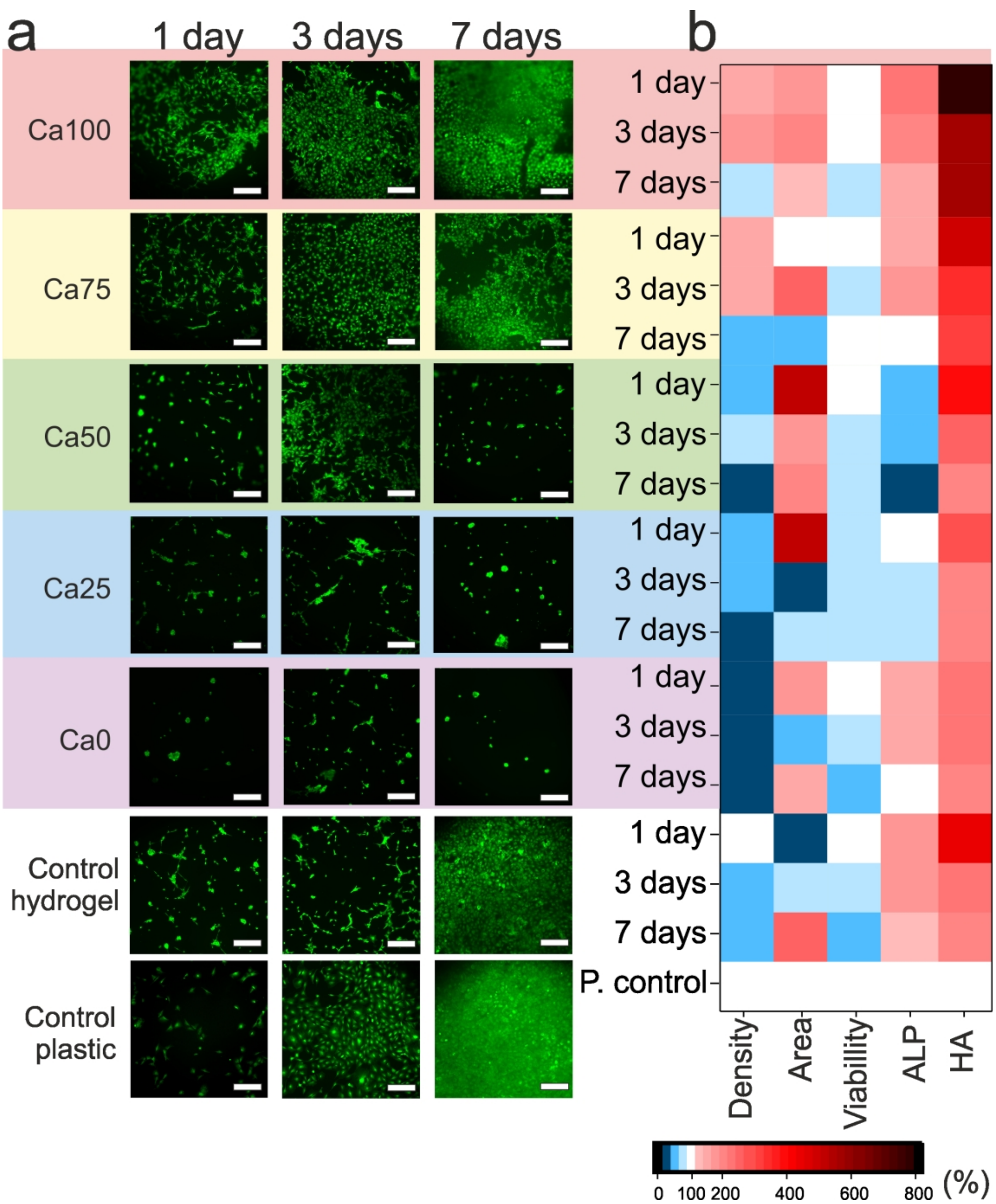

Figure 5. (a) MC3T3-E1 cells cultivated on the surface of the samples mineralized with various concentration of the calcium and magnesium ions (samples from 1to 5), control plastic and control not mineralized hydrogel during 3, 7 and 14 days (calcein, green colour). The scale bar is 200 μm. (b) heat map which represents how the difference parameter deviated from the control. The red is significantly higher than control, and the blue means significantly low then control and the white color represents the 100% control level corresponded to the plastic.

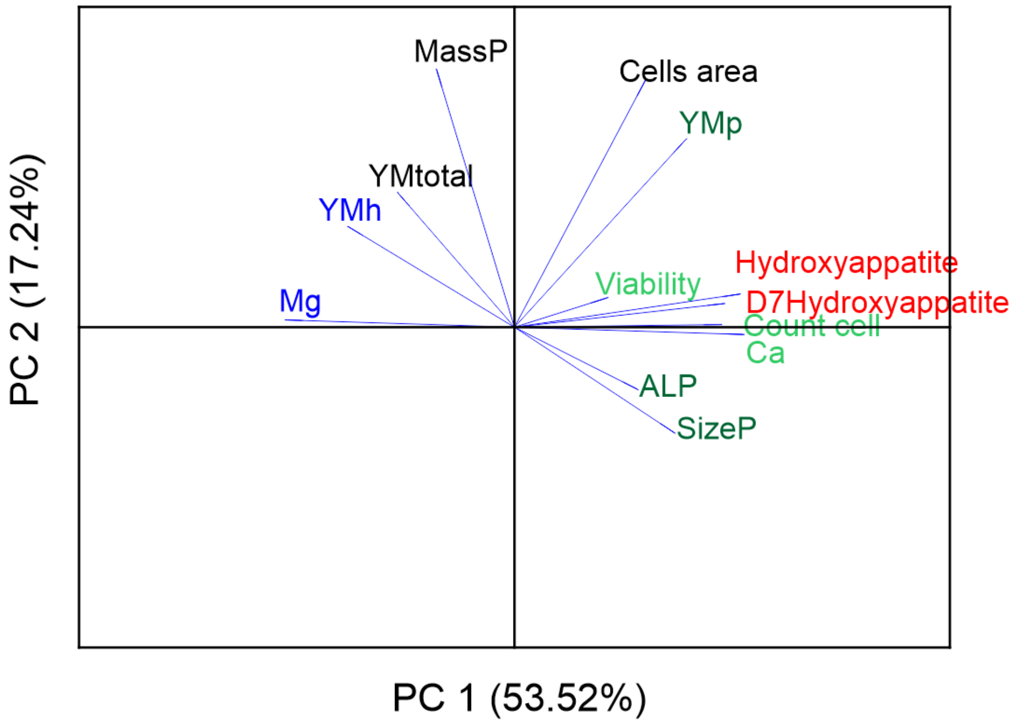

Figure 6. Factors affected by the HA production. Loading plot of the first two PC loading vectors: Mg2+, Ca2+, YmC, YmP, YmH, MassP, Cell area (1 day), viability (1 day), SizeP, ALP (1 day), Density, HA (1 day), HA7 (7 days). The components which repre-sent the amount of hydroxyapatite in a first day (HA) and after the seven day (HA7) are highlighted in red color. The significance of the influence on the factor of interest are highlighted in various colors: significant positive influence (green); negative influ-ence(blue) doesn't have a significant influence (black).

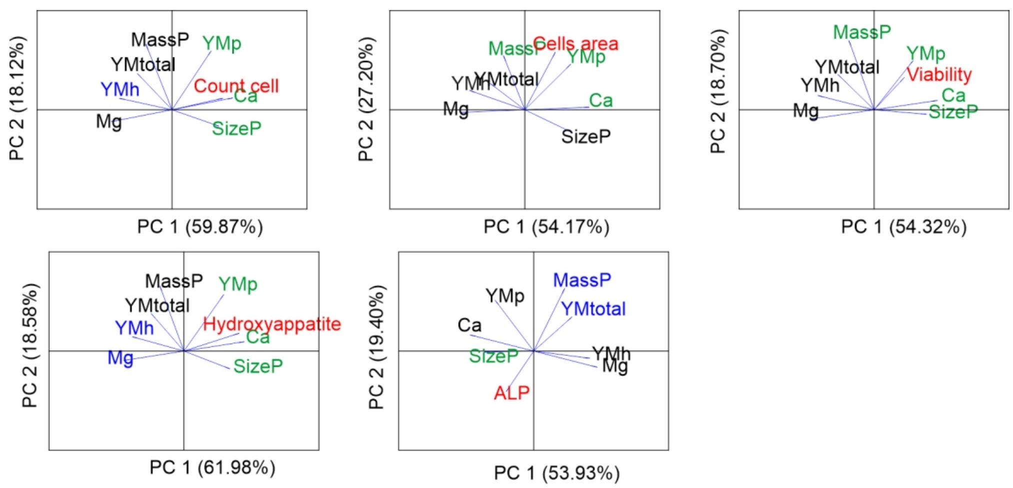

Figure 7. Loading plot of the first two PC loading vectors: Mg2+, Ca2+, YmC, YmP, YmH, MassP, Area, Viability, SizeP, ALP, Density, HA. In red color highlighted the factor of interest. The significance of the influence on the factor of interest is highlighted in various colors: significant positive influence (green); negative influence(blue) doesn't have a significant influence (black).

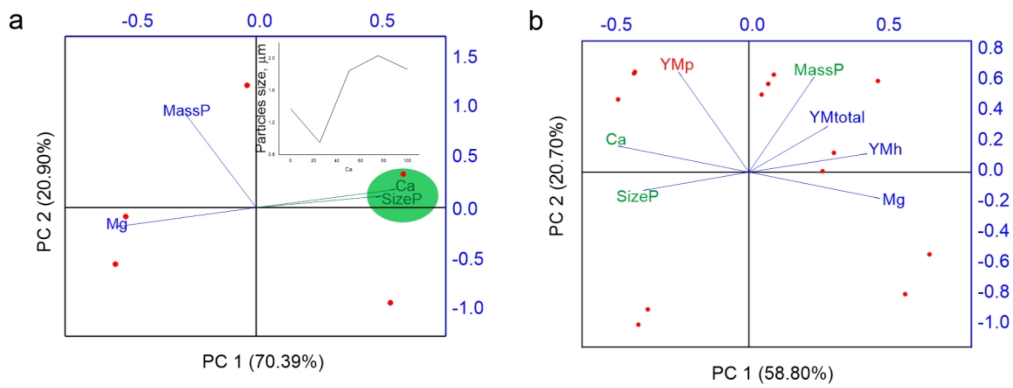

Figure 8. Loading plot of the first two principal component loading vectors: a) Mg2+, Ca2+, SizeP and MassP b) YmC, YmP, YmH, MassP, SizeP, Mg2+, Ca2+. The factor of interest is highlighted in red color. The significance of the influence on the factor of interest is highlighted in various colors: significant positive influence (green); negative influence(blue) doesn't have a significant influence (black). Inset in figure 8a demonstrates the correlation between the particle size and the percentage of calcium ions in the reaction mixture.